Chapter 8

Illuminating Allostery in Metal Sensing Transcriptional Regulators

Nicholas E. Grossoehme and David P. Giedroc

Abstract

The intracellular availability of all biologically required transition metal ions in bacteria, e.g., Zn, Cu, Fe, as well as the detoxification of nonbiological heavy metal pollutants, is controlled at the molecular level by a panel of metalloregulatory or "metal sensor" proteins. Metal sensor proteins are specialized allosteric proteins that regulate the transcription of genes linked to transition metal homeostasis as a result of direct binding of a single metal ion or two closely related metal ions, to the exclusion of all others. In many cases, the binding of the cognate metal ion induces a structural change in a metal sensor oligomer that either activates or inhibits operator DNA binding. A quantitative measure of the degree to which a particular metal drives metalloregulation of transcription is the allosteric coupling-free energy, ΔG_c. In this chapter, we outline detailed spectroscopically derived methods for measuring metal binding affinity, K_{Me}, as well as ΔG_c independent of K_{Me}, presented in the context of a simple coupled equilibrium scheme. Studies carried out in this way provide quantitative insights into the degree to which a particular metal ion is capable of driving allosteric switching, and via ligand substitution, the extent to which individual coordination bonds establish structural linkage of allosteric metal and operator DNA-binding sites.

Key words: Metalloregulation, Metal sensor protein, Metals in biology, Fluorescence anisotropy, Allosteric coupling-free energy

1. Introduction

Allostery encompasses the simple idea that the binding of a ligand at one site can influence the binding or chemical reactivity of the same or different ligand at a distinct, often distant, site. In the classical Monod–Wyman–Changeux or two-state model originally developed for oligomeric proteins or enzymes, initial ligand binding in one subunit triggers a structural change that propagates to other subunits, resulting in a much higher affinity for all other ligands (1). This model is exemplified by the textbook case of heterotetrameric ($\alpha_2\beta_2$) hemoglobin. Here, a structural change is thought to occur in the three empty protomers upon O_2 binding to

a single protomer, resulting in a dramatic increase in O_2 affinity for these subunits. The allosteric activation is such that hemoglobin is thought to be limited to two structural states, which resemble the ligand-free and ligand (O_2)-saturated quaternary structural states. Alternatively, in the sequential model or allostery, individual subunits within an oligomer do not necessarily adapt the same conformation (2). Experimental data for many allosteric proteins are interpreted in the context of one of these two allosteric models.

Transcriptional regulators are specialized allosteric proteins that sense cellular concentrations of metabolites and other small molecular effectors in order to allow for an appropriate response to changing growth conditions. These proteins function through a specific interaction with the operator/promoter region DNA just upstream of the regulated gene or operon. Ligand binding to the protein–DNA complex, typically to a site distinct from the DNA binding site, drives a structural or dynamic change in conformation that modulates the affinity or structure of the regulatory protein–DNA complex. Metalloregulatory proteins are a further subclassification of transcriptional regulators that have evolved to balance the expression of cellular metal uptake and detoxification systems (3, 4). These specialized proteins have evolved from a number of transcriptional regulator families and within a single family, the metal selectivity of individuals can vary significantly. For example, individual members of the ArsR (*ars*enic *r*epressor) family (5) have been described that regulate metal detoxification systems in response to Co, Ni, Cu, Zn, Cd, Hg, Pb, Bi, Sb, or As, via a classical derepression mechanism. In contrast, MerR (*mer*curic ion *r*epressor) family members are known or predicted to function through transcriptional activation mechanism triggered by the binding of Co, Cu, Zn, Ag, Cd, Au, Hg, or Pb (6, 7).

In this methods review, we outline a general spectroscopic method to quantify allosteric regulation of metalloregulatory protein function by metal ions. This methodology is, however, perfectly general and can be extended to investigate ligand-mediated regulation of operator DNA binding by any transcriptional regulatory protein, provided the ligand affinity can be measured directly. When the ligand is a metal ion, multiple spectroscopic approaches are available to accurately measure this affinity (see Subheading 3.4). As presented below, elucidation of the affinity of the protein and the protein–DNA complex for metal ion allows for the direct determination of the coupling-free energy (ΔG_c), a quantitative reporter of the magnitude of the allosteric driving force (8). Alternatively, ΔG_c can be obtained by measuring the DNA binding affinity of apo vs. liganded protein. Depending on the nature of the regulator and characteristics of the system, one approach may well be preferential over the other, but each should give rise to the same value of ΔG_c (9). We first present the generalized coupling scheme and the simple mathematical

construct behind it, followed by common experimental considerations and finally, a detailed description of how to successfully perform and quantitatively analyze the results from these experiments.

1.1. Allosteric Coupling Scheme

The thermodynamic cycle presented in Fig. 1a represents a closed system ($\sum_{i=1}^{4} \Delta X_i = 0$, where X is any thermodynamic state function) that is inclusive of all four possible "end" states that a dimeric metalloregulatory protein (P_2) can adopt in equilibrium with a single DNA duplex operator (D) and n total metal ions (M): apo (P_2), metal-bound ($P_2 \cdot M_n$), DNA bound ($P_2 \cdot D$), and the "ternary" metal–protein–DNA complex (($P_2 \cdot M_n) \cdot D$). Note that P_2 is in equilibrium with free monomer P as well, defined by K_{dimer}, and the model assumes that P has negligible affinity for D. Each side of this thermodynamic box represents a measurable transition between two of the four states (K_1–K_4). This simplistic view of the macroscopic chemical transitions allows for a generic approach to quantify and normalize the allosteric response of a metalloregulatory protein for its DNA binding partner upon metal binding. Note that this scheme can be expanded across the top and bottom equilibria to expressly consider intermediate ligation states with i ligands bound, e.g., where $1 < i < n$; in this case, the macroscopic parameters K_1 and K_2 would be replaced with the appropriate stepwise binding constants (9). Likewise, this scheme can be expanded to include an additional DNA-binding step, and/or oligomeric assemblies larger than dimers (10).

The magnitude of allosteric regulation, K_c, is simply defined as the ligand exchange equilibrium presented (Fig. 1b), where

a

$$2\,P \underset{}{\overset{K_{dimer}}{\rightleftharpoons}} P_2 \; + \; nM \underset{}{\overset{K_1}{\rightleftharpoons}} P_2 \cdot M_n$$

$$+ \qquad\qquad +$$

$$D \qquad\qquad D$$

$$K_2 \Big\updownarrow \qquad\qquad \Big\updownarrow K_4$$

$$P_2 \cdot D + nM \underset{}{\overset{K_3}{\rightleftharpoons}} (P_2 \cdot M_n) \cdot D$$

b

$$P_2 \cdot D \; + \; P_2 \cdot M_n \underset{}{\overset{K_c}{\rightleftharpoons}} P_2 \; + \; (P_2 \cdot M_n) \cdot D$$
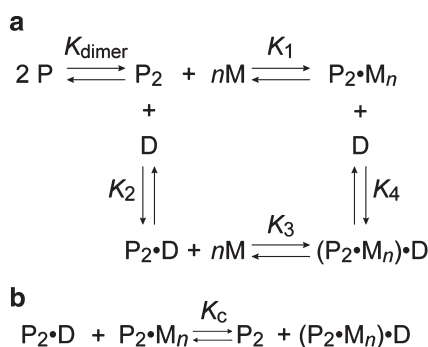
Fig. 1. Allosteric coupling scheme. (**a**) Generalized thermodynamic cycle accounting for the four allosteric "end" states a homodimeric metalloregulatory protein (P_2) can hypothetically adopt apo (P_2), metal-bound ($P \cdot M_n$), DNA-bound apoprotein ($P_2 \cdot D$), and a "ternary" protein–metal–DNA complex (($P_2 \cdot M_n) \cdot D$). Each equilibrium (K_1, K_2, K_3, K_4) describes a direct transition from one configurational state to another as shown. Note also that P_2 and thus the entire scheme is in equilibrium with free P monomer, defined by K_{dimer}, which has no affinity for the DNA (3, 9). (**b**) Ligand exchange equilibrium, defined by the unitless parameter K_c, that dictates the degree of allostery between the metal binding and DNA binding sites (9).

$$K_c = [P_2][(P_2 \cdot M_n) \cdot D]/[P_2 \cdot D][P_2 \cdot M_n] = K_3/K_1 = K_4/K_2. \tag{1}$$

In other words, the allosteric response of a protein is dictated by the stability of the $P_2 \cdot D$ and $P_2 \cdot M_n$ states relative to the $(P_2 \cdot M_n) \cdot D$ and P_2 states. Thermodynamically, this can be thought of as the difference in *metal affinity* between the $P_2 \cdot D$ and P_2 states *or* the difference in *DNA binding affinity* between the $P_2 \cdot M_n$ and P_2 states. Therefore, measurement of K_1 and K_2 or K_3 and K_4 can provide a quantitative determination of the unitless coupling equilibrium constant K_c, which can then be converted to free energy using the standard thermodynamic function

$$\Delta G_c = -RT \ln K_c. \tag{2}$$

For repressors in which metal binding induces dissociation of the repressor of the DNA operator, the $(P_2 \cdot M_n) \cdot D$ state is substantially destabilized relative to $P_2 \cdot M_n$ and free D, and access to the previously occluded promoter by RNA polymerase results in upregulation of the transcription of downstream genes in the operon. In this case, $K_3 < K_1$ (and $K_4 < K_2$) and $\Delta G_c > 0$; that is, the ligand exchange reaction (Fig. 1b) is not favorable and the two biologically relevant "end" states are $P_2 \cdot M_n$ and $P_2 \cdot D$. This is most common for regulation of metal detoxification mechanisms such as *Staphylococcus aureus* CzrA and *S. aureus* pI258 CadC in response to Zn^{II}/Co^{II} and $Cd^{II}/Pb^{II}/Bi^{III}$, respectively (11–13). Alternatively, when $K_3 > K_1$ (and $K_4 > K_2$), $\Delta G_c < 0$ and P_2 and $(P_2 \cdot M_n) \cdot D$ are the two biologically relevant states. In this case, excess cellular metal represses downstream gene transcription by the formation of $(P_2 \cdot M_n) \cdot D$ complex as is the case for the largely Fe^{II} and Mn^{II} sensing Fur family and DtxR family repressors (14–16).

2. Materials

1. A 1-cm pathlength quartz cuvette (NSG Precision Cells, Inc., Farmingdale, NY) is ideal for carrying out spectroscopic measurements. If the spectrometer has a stirring mechanism, magnetic stir bars can be used for optimal mixing. Fluorescence experiments require all four sides of the cuvette to be optically transparent.

2. Reaction buffer is dependent on experimental requirements as discussed in Subheading 3.1. A commonly used buffer is MOPS (2-(*N*-Morpholino)propanesulfonic acid) (>99%) at pH 7.0 and 100 mM NaCl.

3. An extensive collection of fluorescent metal chelating dyes are available from Molecular Probes. Prepare and store 100 μL aliquots of 1–2 mM concentrations as recommended by the manufacturer.

4. To carry out anaerobic experiments, a variety of gastight syringes are available from Hamilton Company (Reno, NV) and cuvettes are commercially available from a variety of suppliers including NSG Precision Cells, Inc. (Farmingdale, NY).

5. Stock metal solutions should be prepared from ultrapure metal salts, e.g., zinc(II) sulfate, lead(II) chloride, cobalt(II) chloride, etc. (Johnson-Matthey) at neutral pH such that the metal salts are stable. For example, Zn^{II} is stable under atmospheric conditions in a wide range of buffers, while Fe^{II} must be prepared and stored under strictly anaerobic or acidic conditions to prevent air oxidation to Fe^{III}. Pb^{II} and Bi^{III} salts must be prepared in a weakly chelating buffer, e.g., bis–Tris, to avoid precipitation of insoluble metal hydroxides (17). We recommend preparing 100 mM metal stocks for use as metal titrants. The metal concentration of these stock solutions are then accurately determined by atomic absorption (18, 19) or atomic emission spectroscopy using National Institute of Science and Technology (NIST) approved standard solutions (Alfa Aesar, Ward Hill, MA) for standard curve calibration.

6. DNA binding assays require a fluorophore covalently bound to one of the strands. Deoxyribooligonucleotides are commercially available in high purity from a number of commercial sources including Operon (Huntsville, AL) and IDT (Coralville, IA). One of the two complementary DNA strands should contain a bright (high fluorescence quantum yield) fluorophore, e.g., fluorescein, covalently attached to the 3′ or 5′ terminus; the complementary strand should be unmodified. Following purification (see Note 1), 100 μM dsDNA stock solutions are prepared from the individual ssDNA by mixing a 1:1 unlabeled:labeled molar ratio of DNA strands. The 10% molar excess of the unlabeled DNA ensures that all labeled DNA (the experimental reporter molecule) is fully complexed, and that there are no unanticipated experimental complications that arise from the slight excess of unlabeled ssDNA. Annealing is accomplished by heating to 95°C followed by slowly cooling to room temperature, with DNA duplex formation confirmed by native polyacrylamide gel electrophoresis. Care must be taken to avoid fold-back intramolecular DNA hairpin structures that might arise from the palindromic or self-complementary nature of the individual ssDNA strands (see Note 2). DNA duplexes prepared in this way are stored in the dark at −20°C and are stable indefinitely.

3. Methods

3.1. Solution Conditions   The selection of appropriate experimental solution conditions is central to any experimental design, since one or more of these variables may dictate the success or failure of an experiment.

1. *pH*. Metals are positively charged ions and thus tend to associate with anionic or neutral ligands; as a result, the protonation state of these ligands can significantly influence the measured affinity of a regulatory protein for a metal ion. Accordingly, a more acidic environment will generally reduce the apparent affinity (K_{app}) according to (3) where K is the pH-independent binding constant and K_H is the macroscopic proton affinity for a ligand. A pH range from 6 to 8 is a common for conducting these experiments.

$$K_{app} = \frac{K}{(1 + K_H[H^+])}. \tag{3}$$

2. *Buffer*. In addition to the major obvious criterion for buffer selection, i.e., to maintain a constant pH, the potential for metal–buffer interactions should also be carefully considered. Very few common biological buffers are actually innocent in this regard and nearly all associate with metal ions to some degree (20). However, several common buffers containing tertiary amines, many of which are derived from the original Good series of biological buffers (21), are very weakly coordinating and span the physiological pH range. These include MES ($pK_a = 6.19$), MOPS ($pK_a = 7.09$), PIPES ($pK_a = 6.77$), and PIPPS ($pK_a = 7.96$) (22). When working with redox active metals, it should also be noted that some buffers promote undesired redox solution chemistry between the metal and buffer. Particularly notable in this regard is HEPES, which should be avoided when studying Cu^{II} interactions in the presence of ligands that stabilize Cu^I, as redox chemistry may well occur (23). Although phosphate buffer has been commonly used to measure protein–metal interactions, this buffer should be avoided as metal-phosphate chemistry is metal-specific, complicated, often unquantified, and typically ignored. Table 1 lists known metal affinities, β_i, for several common biological buffers and chelators; in addition, a unitless competition parameter, Ω, is given for these molecules under one set of standard solution conditions, for illustration. Ω is readily calculated from (4) where L is the deprotonated form of the ligand and β_i is the ith sequential equilibrium constant:

$$\Omega = 1 + \sum_i \beta_i[L]^i. \tag{4}$$

Table 1

Zn^{II}, Ni^{II}, and Cu^{II} stability constants (log β M_iL_k) for common experimental buffers and chelating agents with competition values (Ω) given for common experimental conditions

	βM_iL_k	H+	Zn^{II}	Ni^{II}	Cu^{II}
Tris	ML	8.1	2.24	2.63	4.05
	ML_2			4.5	7.6
	ML_3				11.1
	ML_4				14.1
	Ω (50 mM, pH 8)		5	25	3.2×10^7
Bis–Tris	ML	6.54	2.38	3.59	5.27
	Ω (50 mM, pH 7)		10	145	6,900
HEPES	ML	7.52	n/d[a]	n/d[a]	3.22
	Ω (50 mM, pH 7)				20
EDTA	ML	9.52	16.5	18.4	18.8
	ML_2	15.65			
	Ω (1 mM, pH 7)		8.4×10^{10}	6.7×10^{12}	1.7×10^{13}
NTA	ML	9.46	10.5	11.5	12.7
	ML		14.24	16.3	17.4
	Ω (1 mM, pH 7)		1.0×10^5	1.0×10^6	2.0×10^7

$\beta M_iL_k = [M_iL_k]/[M]^i[L]^k$ where L is the deprotonated form of the indicated substance. All values are NIST reviewed (27) for 100 mM NaCl, 25°C
[a] Values not experimentally determined; however, metal association is likely

3. *Ionic strength.* The apparent affinity measured in metal binding equilibria is dependent upon the concentration of ions in solution (ionic strength, I) according to the Debye–Hückel relationship where

$$I = \frac{1}{2} \sum_i Z_i^2 [\mathrm{i}] \qquad (5)$$

I is a function of the total ionic content and scales with the square of the valency for each species, i.e., 1 μM Fe^{III} ($z = 3$) contributes 9×10^{-6} M while 1 μM Fe^{II} ($z = 2$) contributes 4×10^{-6} M to I. This value directly influences the activity coefficient, and hence the measurable equilibrium constant. However, since typical metal binding experiments with metal sensor proteins are carried out in the 50–500-mM range in monovalent salt concentration (MX, NaCl or KCl), metal salts typically make a negligible contribution to I. Elevated [MX] in these systems is often required to enhance protein solubility and/or ensure that the affinity of protein–DNA interactions are within the measurable range (see Subheading 3.4), the latter given the substantial electrostatic contribution to K_a for

virtually all protein–nucleic acid binding equilibria (24–26). For a direct comparison of binding affinities between different systems, the solution conditions must obviously be identical; a monovalent salt concentration of 100 mM has been widely used for metal binding assays (27) and provides a point of reference for quantitative comparisons of metal–protein affinities.

4. *Temperature*. The experiments outlined below allow measurement of equilibrium constants that are inherently temperature-dependent thermodynamic quantities. While ambient temperature experiments are common, the temperature in standard laboratories can fluctuate over the course of hours or days. Therefore, a mechanism to maintain constant temperature, such as a circulating temperature bath, is necessary. Common experimental temperatures are 25°C or 37°C to mimic ambient or physiological temperatures, respectively.

5. *Oxygen sensitivity*. Intracellular environments are largely reducing, hence the oxidation states of metal ions and surface cysteines tend to be in a reduced state, i.e., Fe^{II} and Cys-SH or Cys-S$^-$ as compared to Fe^{III} and Cys-S–S-Cys. It is therefore necessary to determine the sensitivity of a system to oxygen. For the DNA binding assays (see Subheading 3.4), it may not be necessary to use stringently anaerobic conditions if a strong reducing agent is present in the buffer. These might include dithiothreitol (DTT), dithionite, or tris(2-carboxyethyl)phosphine (TCEP), which are commonly used for this purpose (see Table 2). However, extreme caution is urged when using DTT in the presence of metal ions since many make high affinity metal–DTT complexes (27) that may ultimately out-compete metal–protein interactions, particularly when considering the large molar excess that will likely be present in metal-binding experiments. For these reasons, we routinely perform metal-binding experiments under anaerobic conditions in the absence of reducing agents (see Subheading 3.3).

3.2. Metal-Free Buffers   Since the goal of these studies is to determine the affinity of a protein for a specific metal ion, an undesirable and often overlooked competition from other metals in the buffer needs to be avoided. Adherence to these simple guidelines will ensure the minimization of background metal contamination.

1. *Preparation of glassware*. Standard laboratory glassware is silicate (SiO_2) and simple electrostatics predicts that metal cations will nonspecifically adhere to this anionic surface. This is particularly important for metalloregulatory proteins since many possess extremely high affinity for their cognate metal (26, 28), and thus can potentially "leach" metals from contaminated surfaces. Since protons will out-compete any residual metal

Table 2
Common experimental reducing agents used in metal-binding studies

Reducing agent	$E°$ (mV, pH 7.0)	log β_{ZnL}	log β_{ZnL2}	log β_{Zn3L4}	log β_{ZnHL}
Dithiothreitol	−330[a]	11.1[b]	17.95[b]	50.9[b]	–
TCEP	N/A	2.91	–	–	9.00
Glutathione	−263[c]	n/d[d]	n/d[d]	n/d[d]	n/d[d]
Dithionite	−660[e]	–	–	–	–

β $Zn_iH_jL_k = [Zn_iH_jL_k]/[Zn]^i [H]^j [L]^k$ where L is the deprotonated form of the indicated substance.
N/A, not available
[a]Ref. 54
[b]Ref. 55
[c]Ref. 56
[d]Zn affinity for glutathione is currently not rigorously quantified, although significant affinity is likely via Zn-thiolate coordination
[e]Ref. 57

ions on this surface, all glassware is typically soaked in 1% nitric acid (HNO_3) to significantly reduce residual metal contamination derived from the glassware. Following acid treatment, the glassware should be rinsed exhaustively ($\geq$3 times) with metal-free water (see below) to avoid an unwanted change in the pH buffer solutions.

2. *Metal-free water.* Reverse-osmotic treatment and deionization of water (RODI), standard in most research laboratories, is not sufficient to remove metal ions to the degree required for metal binding assays. Additional metal removal can be provided by numerous standard purification systems that are capable of deionization to a resistance $\geq$18 MΩ cm. Alternatively, strong metal chelators conjugated to solid styrene beads are commercially available, i.e., Chelex, and can be used to treat laboratory grade RODI water in order to produce operationally defined "metal-free" water. This can be accomplished in two ways. The first option is to pass water through a column containing chelating resin and collect in an acid-washed container. Alternatively, the resin can be added directly into the water and shaken for several hours. Separate the phases by centrifugation and careful decanting.

3. *Buffer preparation.* Buffer salts, as provided by the manufacturer, are commonly contaminated with small amounts of divalent metal ions. While very high purity buffer solids can be obtained commercially, removal of residual metal can easily be accomplished by treating the prepared buffer with Chelex, as described just above. Note that Na^+ or H^+ ions (depending on the regeneration protocol used for the Chelex resin) will replace the metals to maintain electrostatic neutrality and,

depending on the amount of metal removed from the buffer, this may be significant. Determination of the pH and conductivity of the buffer solution following Chelex treatment is therefore strongly suggested.

3.3. Anaerobic Preparations

If oxygen reactivity is a concern, additional steps must be taken to ensure a rigorously anaerobic environment since thoroughly degassed or deoxygenated buffers and solutions are required by these experiments.

1. Prepare the buffer solution using metal-free water and remove residual metal as necessary (see Subheading 3.2).

2. Deoxygenate all solvents using one of two standard protocols. The first is a more rapid method (see Note 3) while the second is more thorough and minimizes solvent evaporation (see Note 4).

3. Stock metal solutions should be prepared and stored under an inert atmosphere. The simplest method is to dissolve a known mass of metal salt in an anaerobic chamber (from Vacuum Atmospheres or Coy). If an anaerobic chamber is not available, deoxygenation can be accomplished suboptimally by extensive bubbling of argon or nitrogen from a cylinder of compressed gas through a metal stock solution.

4. The final step is to thoroughly buffer exchange the purified protein into an oxygen-free buffer. Concentrate the protein stock to ~1–2 mL, transfer to an anaerobic chamber, and dialyze at least 4 h in 500 mL of the buffer to be used to metal binding experiments. The dialysis buffer should be exchanged four times to ensure a thorough removal of metal chelators and reducing agents that may have been used during protein purification.

3.4. Metal Binding Assays

Biological function of metalloregulatory proteins is dictated, at least in part, by metal selectivity, which is a governed by the relative affinities for cognate vs. noncognate metal ions (3). Therefore, a quantitative measure of metal affinity can provide critical insight into the thermodynamic driving forces behind these sensors. Using metal binding assays described here, the K_i defined by the two *horizontal* equilibria in Fig. 1a (K_1 and K_3) can be used to determine K_c and ΔG_c using (1) and (2), respectively. However, if $\Delta G_c > 0$, the ternary $(P_2 \cdot M_n) \cdot D$ complex may not be stable under the experimental conditions since M may well dissociate the complex, i.e., shift the equilibrium to $P_2 \cdot M_n$ and free D. As a result, the integrity of the so-formed $(P_2 \cdot M_n) \cdot D$ complex must be independently verified using size exclusion chromatography, for example (9). A good rule of thumb is to employ a concentration of $P_2 \cdot D$ that is ≥ 50-fold larger than $1/K_4$ (see Fig. 1a). A number of spectroscopic approaches are available to measure K_1 and K_3; however, a

number of considerations will dictate which of these approaches are most directly applicable. The examples given assume an aerobic environment is suitable, but nearly all applications are easily adapted for anaerobic conditions using the guidelines discussed (see Subheading 3.2).

3.4.1. Direct Titrations

Under ideal circumstances, a direct titration of metal into protein can provide an isotherm that can be fit to an appropriate binding model to obtain a unique binding constant(s). Requirements for this approach are twofold: (1) the metal of interest must induce a measurable change in the spectroscopic signal, S, e.g., absorbance, fluorescence, or fluorescence resonance energy transfer (FRET); and (2) the apparent affinity must be within a measurable range since K_i is determined by free, not total, metal concentration. For example, Cd^{II} and Pb^{II} binding to *S. aureus* CadC can be directly monitored via intense $S^- \rightarrow Me^{II}$ ligand-to-metal (or metal-to-ligand) charge transfer (LMCT) transitions as a result of metal coordination with cysteine residues with λ_{max} observed at 238 and 352 nm, respectively (18, 29). Alternatively, if there is an endogenous protein-derived fluorophore located near the metal binding site, i.e., Trp or Tyr, metal binding may induce a fluorescent enhancement or quenching of the fluorophore. In this case, measurement of the change in total fluorescence may be used as a reporter for metal binding (30). The optimal experimental concentrations will depend on the molar extinction coefficient and apparent metal affinity for the system under study.

The measurable range of metal affinities can easily be extended to much higher K_i values by the addition of a competing ligand of known affinity, e.g., ethylenediaminetetraacetic acid (EDTA) or nitriloacetic acid (NTA) (see Table 1). This approach requires that a known concentration of competitor ligand is added and the affinity of this ligand be known *under the experimental conditions* of the assay. Such competition experiments can be analyzed using the general approach presented below (see Subheading 3.5) provided one ensures that all relevant equilibria are included in the model. This includes the pH-dependent competition parameter, Ω, which incorporates the effects of pH and ligand pK_a values into the fit. Since the chelator ligand EDTA forms a 1:1 complex with most transition metals, Ω for Zn^{II}-EDTA at 1.0 mM EDTA, pH 7.0 will be used here to illustrate this calculation. In most cases, it is the fully deprotonated form of the competing ligand, denoted L, that forms a stable complex with a metal ion; as a result, one needs to calculate the concentration of free L, [L], from $[L]_{total}$ and other protonated forms of L, denoted H_xL according to (6)

$$[L]_{total} = [L] + [HL] + [H_2L]. \tag{6}$$

For EDTA, the two relevant pK_a values that need to be considered are 9.52 and 6.13. From $K_{H_xL} = 10^{-pK_a}$, one obtains (7), from which [L] can be calculated (8):

$$[L]_{total} = [L] + K_1[H][L] + \beta_2[H]^2[L], \qquad (7)$$

$$[L] = \frac{[L]_{tot}}{1 + K_1[H] + \beta_2[H]^2}. \qquad (8)$$

Note that the denominator in (8) is the binding polynomial of EDTA for protons, denoted Q, when taking free L as the reference state. Substituting into (7) and (8) the known values for EDTA (27), $K_1 = 10^{9.52}$ M^{-1}, $\beta_2 = K_1K_2 = 10^{9.52+6.13}$ M^{-2}, $[H^+] = 10^{-7}$ M and $[L]_{total} = .001$ M, gives $[L] = 3.05 \times 10^{-6}$ M. This value, along with the Zn^{II}-L affinity constant, $\beta_{1,Zn} = 10^{16.5}$ M^{-1} (see Table 2) is input directly into (4) (see Subheading 3.1) to obtain the pH-dependent competition parameter, Ω, at pH 7.0. This gives $\Omega = 8.4 \times 10^{10}$ (see Table 2). This value is then used to calculate the affinity of the protein for metal, K_{Me}, from an apparent equilibrium constant, K_{app}, derived from a fit to the data that does *not* take into account competition with a competitor ligand (see Subheading 3.5), from (9):

$$K_{Me} = \Omega K_{app}. \qquad (9)$$

Alternatively, one can simply calculate a conditional stability constant, K', for the Zn^{II}–EDTA complex which is given by $K' = \beta_{1,Zn}/Q = 9.6 \times 10^{13}$ M^{-1} at pH 7.0. Figure 2 demonstrates the dramatic influence that a competitor ligand, 50 mM Tris in this case, can have on the determination of K_{Me} for a protein–metal complex.

For the method that follows, it is assumed that 20 μM total protein will lead a spectral signal, S, that is readily measured and that S is absorbance.

1. Prepare 1 mL of experimental buffer in a quartz cuvette. Ensure that the cuvette has been acid washed, extensively rinsed with metal-free water and dried with spec-pure methanol, and is free of any optical interferences (such as fingerprints) by cleaning with a Kimwipe. Blank the spectrophotometer over a broad range (200–800 nm).

2. In an optically identical quartz cuvette, prepare 1 mL of 20 μM metal sensor protein.

3. Acquire an initial wavelength scan of the ultraviolet and visible spectral regions (240–700 nm).

4. Prepare a 1.0-mM solution of metal in an identical buffer spiked with 20 μM protein. The addition of protein to the titrant solution avoids the otherwise inevitable dilution of the protein concentration over the course of the experiment.
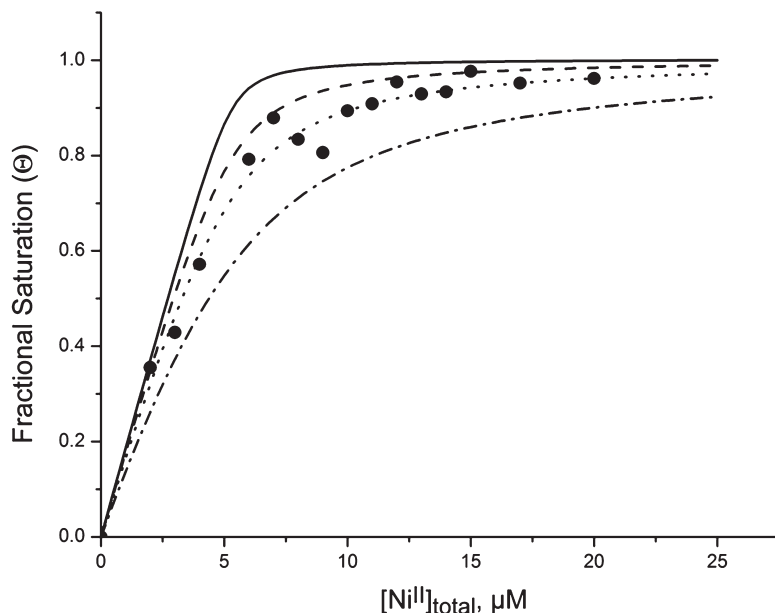
Fig. 2. Representative titrations of a 100-μM Ni^{II} stock solution into Ni^{II}/Zn^{II} binding protein, Tm0439, from *Thermotoga maritime* (*filled circles*) (30). The best fit to this data ($K_{Ni} = 1.47 \times 10^7$ M^{-1}) is shown in the figure as a *dotted line*, which includes competition from the buffering substance, 25 mM Tris, pH 8.0 ($\Omega = 10$). The *solid line* represents a simulated curve that corresponds to the same K_{Ni} but without consideration of buffer competition in the fitting model ($\Omega = 1$), while the *dashed* and *hashed* lines represent competitor concentrations of 12.5 and 50 mM Tris, with the same K_{Ni}. Table 1 compiles relevant competition values for Tris at pH 8.0. Without consideration of Ω, the value of K_{Ni} would be erroneously determined.

This greatly simplifies data analysis since the most simple fitting procedures require a constant protein concentration (see Subheading 3.5). Alternatively, if this is not possible, i.e., excess metal leads to precipitation of the protein, adjust the titrant stock concentration to ensure that the total dilution of the protein over the course of the experiment does not exceed 5–10%.

5. Make a 1–2-μL injection of 1.0 mM metal into the 20-μM protein solution (corresponding to 1–2 μM metal). Allow appropriate mixing time. If a stirring mechanism is not available, manual mixing may be necessary. Note that some metals, such as Ni^{II} and Cu^{I} have very slow ligand exchange kinetics (31). A kinetic experiment may be required prior to the equilibrium titration in order to ensure that adequate mixing time is allowed for the system to come to equilibrium.

6. Scan the UV–vis region. Note small changes in the electronic spectra. LMCT tend to have sizable changes in absorbance due to a high molar absorptivity ($\varepsilon > 1,000$ M^{-1} cm^{-1}); on the other hand, changes in the $d\rightarrow d$ ligand-field region can be

very small given the very low molar intensities of these transitions ($\varepsilon < 200$ M^{-1} cm^{-1}) (32).

7. Repeat the previous two steps until no additional change in S is observed, outside of that expected for dilution.

8. Thoroughly clean the cuvette and repeat the experiment using identical metal aliquots, but in the absence of protein. This titration provides the background signal that can be subtracted point-by-point from the experimental data.

9. These data are commonly presented as absorbance (or molar absorptivity) as a function of wavelength with all aliquots superimposed on the same x, y coordinate. This representation makes it particularly easy to recognize spectral changes as a function of metal concentration.

10. For data fitting (Subheading 3.5), select a wavelength at which maximal change in the absorption spectrum S is observed and plot the S_i as a function of total concentration of added metal titrant.

3.4.2. Surrogate Metal Competition

In some cases, an alternative, or noncognate, metal can be used to determine the binding affinity of the cognate metal ion via a competition experiment. This is particularly applicable when the two metals bind with identical coordination geometries. One common example of this approach is to substitute Co^{II} for Zn^{II} in tetrahedral coordination sites (33). Unlike spectroscopically silent Zn^{II} (d^{10}), Co^{II} (d^{7}) has a distinct and measurable spectroscopic signature which enables direct determination of Co^{II} affinity (see Subheading 3.3.1), with a subsequent competitive displacement of Co^{II} by Zn^{II} (34). The experimental details laid out below assume that Co^{II} is used as the surrogate reporter metal for Zn^{II}.

1. Carry out a $Co^{II} \rightarrow$ protein experiment as described above (see Subheading 3.3.1). Determine the Co^{II} affinity using the data fitting procedures in Subheading 3.5. This is often straightforward because $K_{Co} \leq 10^7$ M^{-1} for many Co^{II} binding sites and a direct titration generates a change in signal S that is nonstoichiometric in the protein concentration range suitable for measurement (20–50 μM).

2. Prepare a 1-mL solution of 20 μM protein and 100 μM Co^{II} in a clean quartz cuvette. The concentration of protein and Co^{II} can be adjusted to optimize S. If the affinity for Co^{II} is high enough, stoichiometric equivalence may be adequate. Blank the spectrophotometer over a broad range.

3. Prepare a solution containing 1.0 mM Zn^{II}, 100 μM Co^{II}, and 20 μM protein. Note that if the concentrations of Co^{II} and protein are adjusted in the previous step, they should be adjusted here as well. This is to ensure that Zn^{II} is the only variable throughout the metal-displacement experiment.

4. Make 1–2 µL injections of Zn^{2+} into the 1-mL protein solution. Allow adequate mixing time. Co^{2+} and Zn^{2+} both have rapid ligand exchange kinetics (31); however if the metal binding site is buried, this can severely impair the exchange. Upon equilibrium, scan the UV–vis region and monitor changes in the spectra. The expected response is directly reverse as the surrogate metal addition.

5. Repeat the previous step as necessary until an adequate baseline is reached. Note that full displacement of the spectroscopically active metal is not necessary to provide a complete data set for rigorous fitting.

6. Clean the cuvette and repeat the experiment in the absence of protein. This provides a point-by-point background for subtraction from the experimental data.

3.4.3. Spectroscopically Active Metal Chelators

In many situations, it may not be possible to use a surrogate metal as a spectroscopic reporter or monitor metal binding directly. In these cases, metal chelators with known metal affinities and sensitive spectroscopic signatures are available that can be used to determine the metal affinity, K_{Me}, for the sensor protein. This type of competition experiment is based on the relative affinities of the metal (Me) for the chelator (C (10)) and for the protein (P (11)).

$$Me + C \rightarrow Me \cdot C \qquad K_b \qquad (10)$$

$$Me + P \rightarrow Me \cdot P \qquad K_{Me} \qquad (11)$$

Since these two equilibria will be in direct competition over the course of this experiment, selection of chelator characterized by an appropriate K_b is critical to the experimental design. Note that this experiment is exactly analogous to the ligand (L) competition experiment discussed above (see Subheading 3.3.1), except the change in S is coming from the ligand C rather from P. As shown in Fig. 3, there is a dynamic range of K_{Me} over which each chelator probe is applicable. When $K_{Me}/K_b < 0.01$, the protein does not effectively compete with the chelator for metal binding and the titration curve is not distinguishable from a direct titration of metal into the free chelator. Alternatively, when $K_{Me}/K_b > 100$, a unique fit for K_{Me} cannot be obtained due to lack of competition from the chelator (35). For example, mag-fura-2 has an estimated affinity of $K_b = 5.0 \times 10^7\ M^{-1}$ for Zn^{II} (pH 7.0 and 25.0°C) (36) and can also be used for a range of divalent cations since their affinities have been measured (37). In the case of Zn^{II}, this results in a measurable range of Zn^{II}–protein affinity of $5 \times 10^5\ M^{-1} < K_{Me} < 5 \times 10^9\ M^{-1}$. For higher affinity interactions, quin-2 can be used since it has a much higher affinity for Zn^{II} ($K_b \approx 2.7 \times 10^{11}\ M^{-1}$) (38) which extends the dynamic range over which K_{Me} can be measured by this technique to $\geq 10^{13}\ M^{-1}$
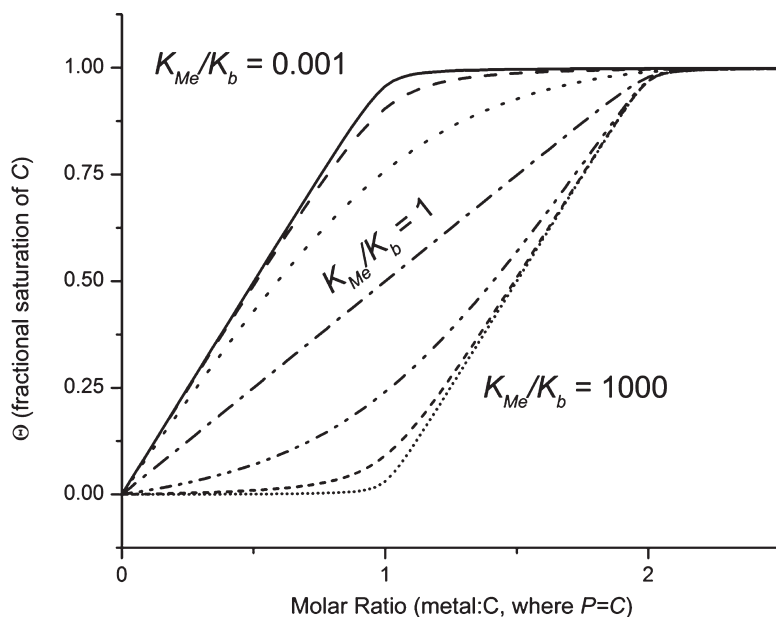
Fig. 3. Simulated data for the titration of a metal into a equimolar solution of protein and spectroscopic metal chelator. Each line corresponds to a tenfold change in the K_{Me}/K_b ratio, as described in (4) and (5). When $K_{Me}/K_b < 0.01$, the protein does not effectively compete with the chelator and the titration cannot be distinguished from a direct metal $\rightarrow$ chelator titration. When $K_{Me}/K_b > 100$, the chelator does not effectively compete with the protein. In both of these cases, a unique fit to the experimental data cannot be obtained.

(39). Note that parallel experiments done under the same solution conditions should provide internally consistent values of K_{Me} (40). Lower affinity chelators are also commercially available (Molecular Probes); however, metalloregulatory proteins tend to make specific and high affinity interactions with the metals that they sense. Although the experimental protocol described below assumes that the Zn^{II} affinity will be determined by mag-fura-2 competition, the approach is perfectly general and can be used directly with other metals or chelators.

1. Blank the spectrophotometer with the experimental buffer prepared in a clean quartz cuvette.
2. Prepare a 1.0-mM Zn^{II} solution in the experimental buffer.
3. Prepare 1 mL of 20 μM mag-fura-2 in a clean quartz cuvette (lower concentrations of 1–5 μM can be used in the fluorometer). Measure the absorbance minimally from 300 to 400 nm.
4. Make a 1–2-μL injection of Zn^{II} into the mag-fura-2 solution. Allow 1–2 min for mixing or sufficient time for S to stabilize. If mechanical mixing is not available, gently aspirate the solution with a micropipette. Measure S over the same spectral window.

5. Repeat step (4) until no further change is observed. The absorbance at 325 nm is maximal when Zn^{II} is bound to the chelator and minimized at 366 nm when the chelator is not metallated. These data can then be globally fit to a single equilibrium binding model (see Subheading 3.5) to determine K_b.

6. Blank the spectrophotometer with the experimental buffer prepared in a clean quartz cuvette.

7. In a clean quartz cuvette, prepare a 1-mL solution of 20 µM mag-fura-2 and 20 µM protein in the appropriate experimental buffer. Repeat steps (3)–(5). Using K_b determined from the direct titration of Zn^{II} into mag-fura-2, these data can be fit to a simple competition model to fit for K_{Me} (see Subheading 3.5).

3.5. DNA Binding Assay

Fluorescence polarization (P) or anisotropy (r) experiments are most commonly used to determine the affinity of a metalloregulatory protein for duplex DNA operator sequence (41). This hydrodynamic approach, which reports on the size and shape of molecules, utilizes vertically polarized light to selectively excite a subpopulation of fluorophores. The emission intensity is subsequently measured through a polarizer and mathematically translated to anisotropy, r, based on the intensities of horizontally and vertically polarized emission (42). The experiments described in this section provide a guide to determining the vertical equilibria in Fig. 1 (K_2 and K_4). We note however, that for large values of $|\Delta G_c|$, it can be challenging to measure the DNA-binding affinity of the apo (for $\Delta G_c < 0$, or allosteric activation) or the $P_2 \cdot M_n$ complex (for $\Delta G_c > 0$, or allosteric inhibition), since K_2 or K_4, respectively, may be very small or difficult to distinguish from nonspecific binding. In the case of allosteric inhibition, our experience is that it is usually possible to measure K_4 provided high protein concentrations are achievable in the cuvette (≥ 10 µM) (43), and excess total metal (0.05–0.1 mM) can be added to the solution without precipitation of the protein. This ensures that all metal sensor is in the $P_2 \cdot M_n$ form which allows for direct determination of K_4 (see Fig. 1). In order to minimize non- or weakly specific binding of the metalloregulatory protein to adventitious or cryptic binding sites on the DNA, the use of a dsDNA of the minimal length that retains all of the known or projected intermolecular contacts that maximize binding energy is desirable (41, 44); even under these conditions, however, the binding of additional dimers to the dsDNA may not be avoidable (9).

The length of the operator-containing duplex DNA also impacts the ability to easily use a change in r as the basis of detection of protein binding. Longer dsDNA molecules are characterized by a larger intrinsic anisotropy, r_o, with the change in r smaller over the course of the experiment; this will necessarily result in larger error in data fitting. The minimal length requirement of a dsDNA that

maintains high affinity binding varies with each metalloregulator; a DNase I footprint, if available, can be used as a guide for duplex DNA design (26). Alternatively, carrying out binding experiments with a collection of oligonucleotides of incrementally shorter lengths can provide a direct indication of the minimal length as well (43). A 28–32 base pair duplex is, however, a reasonable starting point for most dimeric metalloregulatory proteins for which high resolution structures are known or predicted from functional orthologs (4). The experiment described below assumes a fluorescein-labeled dsDNA.

1. Ensure the spectrofluorometer is configured to measure anisotropy. Polarizers are needed for excitation as well as emitted light. For fluorescein, a 530-nm cut-off filter is often used to remove background light scatter from incident radiation.

2. In a four-sided quartz cuvette, prepare 2 mL of 4–10 nM fluorescein-labeled dsDNA in a appropriate experimental buffer. If a stirring mechanism is equipped, insert a clean magnetic stir bar in the cuvette.

3. Prepare a 2-μM sample of protein in an identical experimental buffer.

4. Measure the anisotropy of the DNA duplex. A typical intrinsic or starting anisotropy (r_o) for a fluorescein-labeled ≈30 base pair duplex dsDNA is ≈ 0.11. Single-stranded DNAs of this length will have r_o ≈ 0.07, with longer duplexes often $r_o \geq 0.15$. We note that r_o is strongly dictated by the nature of the fluorophore and is also influenced by the degree to which the probe intercalates or stacks against the end of the DNA helix, with r_o values of ≥ 0.2 for many commonly used fluorescent dyes (Cy5, Cy3, rhodamine derivatives, coumarin, etc.) (44–46).

5. Add 1–2 μL of 2-μM protein stock. Stir for at least 1 min to allow adequate mixing. Measure the anisotropy once the signal stabilizes.

6. Repeat step (5) until no change is observed. Avoid addition of >200 μL (10%) as fluorophore concentration is considered to be a constant in simple fitting algorithms. Alternatively, 10 nM labeled dsDNA can be added to the 2-μM protein solution to avoid the effects of dilution.

7. Plot r_i as a function of total protein concentration as shown in Fig. 4 (see Note 5). Fit these data to an appropriate model as outlined below and extract a value for K_2 (see Subheading 3.5).

8. Repeat steps (1)–(7) using a preloaded metallated sensor stock as the titrant ($P_2 \cdot M_n$). If the affinity of the sensor protein for metal when bound to DNA (K_3 in Fig. 1) is low, an excess of the same metal salt (50–100 μM) can be added to the binding
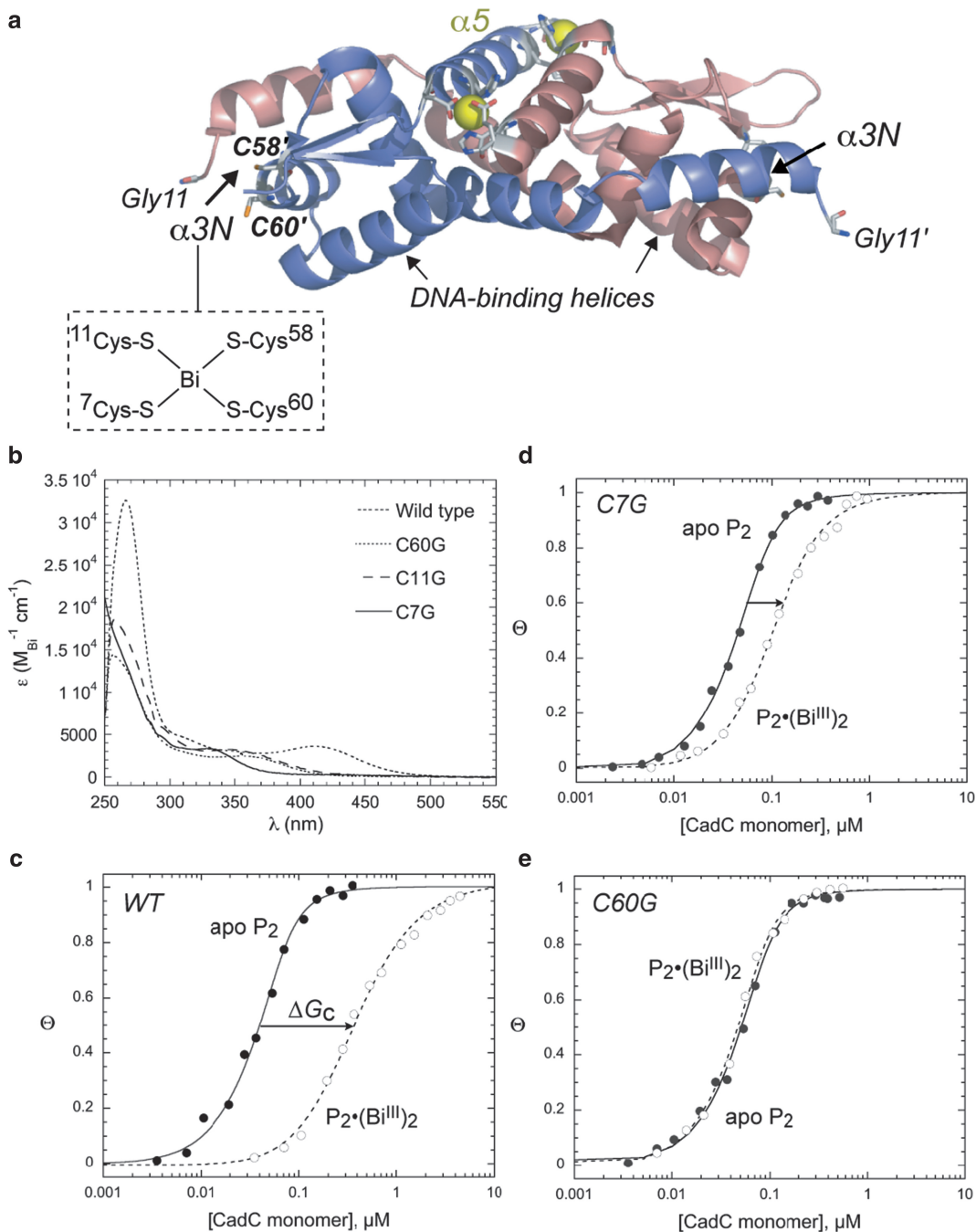
Fig. 4. Representative example of the elucidation of the residue-specific contributions of individual cysteine residues to the allosteric coupling-free energy, ΔG_c. (**a**) Ribbon representation of the crystallographic structure of apo-C11G CadC (residues 11–117 or 11–119), with structural Zn^{II} ions bound in the nonregulatory (18) $\alpha5$ sites (*yellow spheres*) (48). One protomer is shaded *salmon* and one is shaded *blue*, with the empty regulatory Cys_4 $\alpha3N$ sites and the putative DNA-binding helices on each protomer indicated. Bi^{III} is known to form a four-coordinate S_4 complex (47), while Cd^{II} forms a distorted S_4 complex (18, 29) with Cys11 weakly coordinated (49), while Pb^{II} adopts a trigonal planar complex that excludes coordination by Cys11 (18). (**b**) Molar electronic absorption spectra of the stoichiometric Bi^{III} complexes formed

experiment such that $[\text{Me}]_{\text{total}} \geq 10 \times 1/K_3$ thus ensuring that $P_2 \cdot M_n$ is the only form of P_2 in the binding reaction. These steps allow for the determination of K_4, the affinity of the $P_2 \cdot M_n$ for the DNA operator. With K_2 and K_4 in hand, ΔG_c can be determined directly using (1) and (2) above.

The results of experiments of this kind for the $\text{Cd}^{\text{II}}/\text{Pb}^{\text{II}}/\text{Bi}^{\text{III}}$ sensor CadC encoded on the extrachromosomal *S. aureus* pI258 plasmid (47) illustrate the power of this approach to yield detailed insights in the structural basis of allosteric linkage between a metalloregulatory Bi^{III} site and the DNA-binding site. Bi^{III}, like other large thiophilic metal ions Pb^{II} and Cd^{II}, bind to a pair of twofold symmetric Cys-thiolate-rich metal sites at the periphery of the dimer, which we term α3N (Fig. 4a). Bi^{III} binds stoichiometrically to wild-type CadC, like Cd^{II} and Pb^{II} (18), and inspection of the electronic absorption spectrum reveals a four-coordinate S_4 complex composed of Cys7′ and Cys11′ from the N-terminal arm of one subunit (not observed in the crystallographic structure of apo-CadC) (48), and Cys58 and Cys60 in the α3 helix of the other subunit. Substitution of each of the four Cys, one at a time to a nonliganding Gly or Ser residue results in the loss of one Bi^{III}-thiolate coordination bond (Fig. 4) (49); however, each mutant binds Bi^{III} stoichiometrically under these conditions, $K_{\text{Bi}} \geq 10^9$ M^{-1} (data not shown) (47). Knowledge of K_{Bi} allows one to determine the affinity of the wild-type and mutant apo-CadC and Bi^{III}-CadC complexes for a 34-base pair *cad* operator-containing DNA in an effort to determine the degree to which individual metal–thiolate coordination bonds drive allosteric regulation (Fig. 4c–e), with the fitting parameters compiled in Table 3. These results make the striking finding that Cys7 from the N-terminal arm, and most profoundly Cys60, play important roles in metalloregulation in this system, given ΔG_c values significantly smaller than wild-type CadC (18, 47). In contrast, Cys58 and Cys11 play only accessory roles, although the degree to which

Fig. 4. (continued) by wild-type, C7G, G11G, and C60G as indicated. A comparison of these spectra to those of S_3 and S_4 model coordination complexes reveals that wild-type CadC forms an S_4 complex, while the mutant spectra are as expected for the loss of a single thiolate ligand in each case (47). (**c**–**e**) Representative binding isotherms obtained for wild-type CadC (**c**), C7G CadC (**d**), and C60G CadC (**e**) as apoproteins or preloaded with stoichiometric Bi^{III} and 20 nM fluorescein-labeled 34-bp *cad* operator DNA fragment (47). The *solid lines* represent fits to a CadC dissociable dimer-binding model (see Subheading 3.5), with K_{dimer} fixed at the values determined from analytical equilibrium ultracentrifugation under the same solution conditions and K_2 (for apo-CadC) or K_4 (for Bi^{III}-loaded CadC) (see Fig. 1) optimized during the fit (29, 47). Cd^{II} has at most a twofold effect on K_{dimer} (29). Solution conditions: 10 mM Bis–Tris, pH 7.0, 0.4 M NaCl, 1 mM DTT, 25.0ºC with 50 μM EDTA added to the apo-CadC titrations only. $\Theta = (r_i - r_0)/(r_{\text{complex}} - r_0)$, where r_i is the measured anisotropy after each addition of protein titrant (expressed in monomer CadC units), r_0 is the starting anisotropy of the free DNA, and r_{complex} is the fitted value for the saturated $P_2 \cdot D$ complex. r_0 for a duplex of this number of base pairs should be 0.13 (±0.01), with the total change in signal ($\Delta r = r_{\text{complex}} - r_0$) ranging from ≈0.020 to 0.025 for a 27.6-kDa dimer–34-bp DNA complex (≈50 kDa total) (18, 47).

Table 3
Thermodynamic parameters that define the negative allosteric regulation of wild-type and mutant *S. aureus* pI258 CadCs by various metal ions[a]

CadC variant	K_2 ($\times 10^9$ M^{-1})[b]	K_4 (Bi^{III})[b] ($\times 10^9$ M^{-1})	ΔG_c (Bi^{III}) (kcal/mol)	ΔG_c (Cd^{II}) (kcal/mol)	ΔG_c (Pb^{II}) (kcal/mol)
Wild type	1.1 ($\pm$0.2)	0.0067 ($\pm$0.0006)	3.0 ($\pm$0.2)	3.2 ($\pm$0.1)	3.4 ($\pm$0.2)
C7G	0.83 ($\pm$0.06)	0.072 ($\pm$0.009)	1.5 ($\pm$0.1)	1.2 ($\pm$0.2)	0.9 ($\pm$0.1)
C11G	0.58 ($\pm$0.05)	0.021 ($\pm$0.004)	1.9 ($\pm$0.2)	2.8 ($\pm$0.2)	3.4 ($\pm$0.3)
C52G[c]	1.0 ($\pm$0.3)	0.0073 ($\pm$0.0008)	2.9 ($\pm$0.2)	3.3 ($\pm$0.3)	3.4 ($\pm$0.4)
C58S	0.11 ($\pm$0.02)	ND	ND	2.7 ($\pm$0.6)	1.8 ($\pm$0.2)
C60G	1.0 ($\pm$0.6)	1.0 ($\pm$0.1)	0 ($\pm$0.3)	0.1 ($\pm$0.4)	0 ($\pm$0.4)

[a] Data taken from refs. 18, 47
[b] Fitted parameters from the binding curves shown in Fig. 4 with each K_i corresponding to those in the linkage scheme shown in Fig. 1
[c] Cys52 is not conserved in other CadCs (18) and is not a ligand to the metal ion in any case, and thus represents a control substitution. ΔG_c determined using eq vv with $T = 298.15$ K

each contributes is clearly metal-ion dependent (Table 3). This reflects the distinct coordination complexes formed in each case, which is a function of both the charge, size, and specific character-istics of the ions. In fact, Bi^{III} is the only metal for which substitution of Cys11 results in an attenuated ΔG_c; for Pb^{II}, which forms an S$_3$ complex that excludes Cys11 from the coordination sphere (18) and Cd^{II}, which forms a weak coordination bond to Cys11 (49), the C11G substitution is functional silent in vitro and in vivo. Substitu-tion of Cys60 in particular, effectively uncouples metal binding from DNA binding ($\Delta G_c = 0$ kcal/mol), despite the fact that a stoichio-metric metal complex is formed in each case (Table 3).

3.6. Data Fitting Using Nonlinear Least Squares Methods

A number of programs are available that are capable of analyzing spectroscopic data to obtain parameters of interest. In the following discussion, we briefly illustrate the use of DynaFit (50) (http://www.biokin.com/dynafit/), a program free to academic users that utilizes a Levenberg-Marquardt "least squares" method to produce estimated parameters from a set of experimental data. The program utilizes a simple symbolic notation in a script or text file to completely define a chemical equilibrium model through a collec-tion of stacked equilibria, and thus does not require that the user-defined closed-form expression that fully encompasses the model. These script files can be as simple (a single chemical equilibrium) or as complex as required by a model. Once the model is set up, it is important that the user consult the cross-correlation matrix if solving for multiple estimated parameters, since all parameters

that are optimized will be correlated (or anticorrelated) to some degree (51) (see Note 6). Here, we focus on the appropriate mechanisms to generate estimates of binding constants for simple (direct, no competition) and complex (competition) data sets.

It is also important to point out that the user recognize that, like all programs of this type, it is assumed that the change in signal S_i is directly proportional to a fractional saturation, Θ, of the macromolecule from which S derives, i.e., the relationship between S_i and Θ is linear:

$$\Theta = (S_i - S_o)/(S_{complex} - S_o)Z \qquad (12)$$

where S_o is the signal from the free or uncomplexed macromolecule, and $S_{complex}$ is that associated with a saturated complex. This may not be the case (see an example of Ni^{II} binding to the zinc metalloregulator, *Synechococcus* SmtB in ref. 39), but well-established methods are available that can be used to verify a linear relationship, or if not, explicitly define the relationship using a general method of analysis (52). Although there is no reason to believe, a priori, that the incremental change in the anisotropy of the fluorescence is linearly dependent on fractional saturation by bound sensor protein, we have found in at least one case that this is indeed the case, as determined under solution conditions where the DNA-binding is stoichiometric (26).

1. *Units.* When preparing a script file for DynaFit, a common error occurs in the units. Ensure that the concentration units used throughout the script file matches those used in the data file. For example, the *x*-axis of Fig. 4 is µM monomer protein, therefore the concentration of dsDNA must be scripted in µM and the resulting binding constant will have units of μM^{-1}. In this case, a least-squares fit that generates $K = 0.1 \ \mu M^{-1}$ corresponds to $K = 1 \times 10^5 \ M^{-1}$.

2. *Response.* Each independent chemical species that generates a measurable signal, S, i.e., unbound dsDNA labeled with a fluorescent probe, as well as the protein–DNA complex, must be included in the response of the script file. The magnitude of the response is dictated by the individual experiment weighted by the concentration. For example, in the fluorescence polarization experiments shown in Fig. 4, the anisotropy of the fluorescein-labeled 34-base pair duplex DNA (D) (r_o) is ≈ 0.125 while that for the protein–DNA complex ($r_{complex}$) is ≈ 0.145. The total concentration of dsDNA is 20.0 nM (0.02 µM) in each case; this gives response factors of $r_i/0.02$ of 6.25 and 7.25 for the free DNA and the saturated protein–DNA complex, respectively.

3. *Mechanism.* The mechanism is the actual chemical equilibrium model that describes the binding experiment. DynaFit is capable of fitting data to a theoretically infinite number of coupled equilibria, and obviously many different mechanisms (or models) can adequately describe a given data set. Therefore, existing information regarding the system as well as chemical intuition are needed to guide the data fitting process. For a simple one-site model in which apoprotein binds to a ligand, e.g., P_2 binding to D to form a 1:1 complex, the mechanism input into DyanFit is

$$P + D <==> PD : K1 \text{ assoc.}$$

where P is protein dimer P_2 (note this is one-half the total monomer concentration that is directly measured by UV-absorbance, and assumes a nondissociable dimer), D is DNA, PD is the $P_2 \cdot$DNA complex, and K1 is the association equilibrium constant (as designated by assoc.).

4. Most metalloregulatory proteins are homodimers and likely only interact with dsDNA in this form (see Fig. 1a). However, the monomer–dimer equilibrium (defined by K_{dimer}) may come into play if the total protein monomer concentration is used in the experiment $[P]_{total} \leq 1/K_{dimer}$. In this case, the value of K_{dimer} must be known under the same solution conditions from an independent experiment, e.g., analytical equilibrium ultracentrifugation (29, 53), and used as a fixed parameter in a fitting algorithm that explicitly incorporates this linkage as an additional line of script in the mechanism. We refer to this mechanism as the "dimer-linkage model":

$$P + P <==> P2 : K1 \text{ assoc.}$$

$$P2 + D <==> P2D : K2 \text{ assoc.}$$

If K_{dimer} is not known, one can use the same script file and set K1 assoc. to a very large value (e.g., $10^6 \ \mu M^{-1}$); this has the effect of assuming a nondissociable dimer in the fit. Both K_1 and K_{dimer} cannot be simultaneously optimized because the two parameters are nearly infinitely inversely correlated (see Note 6). It is sometimes possible to detect linkage to the monomer–dimer equilibrium (although the extent of that linkage cannot be determined; see Note 5) because the binding curve will appear detectably sharper (more sigmoidal) than a binding curve that is not linked to the equilibrium, due to the fact that $[P]_{total} > 1/K_{dimer}$. This is in fact apparent in the binding curves shown in Fig. 4c–d. Note how the apo-P_2 binding curve is "sharper" than the $P_2 \cdot Bi^{III}$ curve; this is entirely due to the fact that in the former case $[P]_{total} < 1/K_{dimer}$, while in the metallated complex, $[P]_{total} \approx 1/K_{dimer}$.

5. In more complex systems, such as titrating Zn^{II} into a mixture of mag-fura-2 and protein (Fig. 3), the mechanism must include two equilibria that describes Zn^{II} binding to each of the potential ligands.

$$P + Z <==> PZ : K1 \text{ assoc.}$$

$$M + Z <==> MZ : K2 \text{ assoc.}$$

In this example, P is the protein monomer concentration, Z is Zn^{II}, M is mag-fura-2, while PZ and MZ are the 1:1 Zn^{II}–protein monomer and mag-fura-Zn^{II} complexes, respectively. When scripting this mechanism, the two response elements are M and MZ since PZ is optically transparent; K2 is directly determined from a background experiment (see Subheading 3.3.3). Therefore, the only variable is K1, which directly competes with K2 for the binding of Zn^{II}. We note that for most metalloregulatory proteins, metal complexes bridge subunits of dimers or tetramers (4); in this case, P monomer does not actually bind metal to any appreciable degree. As a result, this script has the effect of fitting for two *identical and independent* binding sites on P_2 or more generally *n* such sites on a *n*-oligomeric sensor (10). A more detailed mechanism (or model) that takes these linkages into account can be used to detect negative cooperativity of binding metal ions to a homodimer (32, 44), and is shown below.

$$P + P <==> P2 : K1 \text{ assoc.}$$

$$P2 + Z <==> P2 \cdot Z : K2 \text{ assoc.}$$

$$P2 \cdot Z + Z <==> P2 \cdot Z2 : K3 \text{ assoc.}$$

$$M + Z <==> MZ : K4 \text{ assoc.}$$
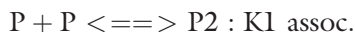
In the case of negative homotropic cooperativity, K3 < K2. Note this scheme can be readily expanded to include the binding of additional metal ions.

4. Notes

1. Synthesis of DNA oligonucleotides on the 200-nmol scale is sufficient to generate adequate material for these experiments. We routinely further purify DNAs by denaturing PAGE followed by electroelution ($l > 20$ nts) or high-resolution anion exchange chromatography ($l \leq 20$ nts), and ethanol precipitation. In the case of denaturing PAGE-purified DNAs, complete removal of acrylamide and urea is ensured by a final reverse phase clean up step using prepacked C18 columns (Alltech) and elution with 50% methanol. Dry to completeness with a speedvac.

2. Some duplex DNA operator sequences are highly palindromic, in which case a ssDNA hairpin may be thermodynamically favored over dsDNA. Annealing under high salt concentration (0.5–1 M NaCl) promotes duplex formation. Additionally, increased strand concentration may be needed to favor the intermolecular complex formation. Note that rapid cooling should be avoided as this process favors hairpin formation.

3. Transfer/prepare the buffer in a 2–3-L round-bottomed vacuum flask (a reaction flask from Kontes works well for this purpose). Attach the flask to a dual line manifold with one dedicated vacuum line and the other attached to a cylinder of argon. Situate the flask on a magnetic stirring mechanism and stir under high vacuum for at least 1 h/L of buffer (2 h/L is recommended). Back-fill with argon for transfer to an anaerobic chamber. Note this method will lead to a small increase in buffer concentration as a result of unavoidable solvent evaporation.

4. Prepare the buffer in a vacuum flask (typically available up to 500 mL) leaving at least 1/3 of the flask volume empty. Submerge the flask into liquid nitrogen or an isopropanol–dry ice slurry until completely frozen. While still frozen, expose to a high vacuum for 10–20 min. Close the flask and warm until completely melted. Submersion in tepid water can help this process; however, caution is urged to avoid fracturing the glassware as a result of a rapid temperature change. Repeat this process three times followed by backfilling the flask with Argon for transfer to an anaerobic chamber.

5. Note that Fig. 4 is plotted on a log [CadC monomer] scale which *visually* expands the range of total [protein] used in these experiments. Data fitting should done on a linear scale since a Gaussian distribution of error assumed by these methods does not scale with logarithmic functions.

6. The degree to which two parameters are correlated or anti-correlated is quantified in the cross-correlation matrix associated with any fitting mechanism or model. For example, in the dissociable dimer model discussed above, the cross-correlation coefficient for K1 (K_{dimer}) and K2 (P_2 DNA-binding affinity) is −0.89 which reflects nearly complete inverse correlation. This means that unique values of K1 and K2 cannot be extracted from the fit, since changing K1 by tenfold and reducing K2 by tenfold will give an imperceptible change in the "goodness of fit" (a χ^2-value). A cross-correlation coefficient of 0 means that the two parameters are independent of one another, with a range of −1 to 1 (51).

5. Conclusions

The experimental approach described here outlines a general strategy to experimentally determine the allosteric coupling-free energy, ΔG_c, for any ligand-modulated transcriptional regulator by measuring the DNA-binding affinity of apo-metallated forms of the protein or, alternatively, the metal binding affinity of apo vs. DNA-bound protein (Fig. 1) (9). The approach therefore takes advantage of the ability to measure defined equilibria independently under one set of solution conditions without complications from competing equilibria within a complex linkage scheme. A detailed discussion of how to conduct these experiments is presented, along with consideration of the particular challenges associated with the study of transition metal ions as allosteric ligands. It should be stressed that the nature of the solution conditions required by these titrations can have an enormous impact on the information content of these experiments, and in most cases, can only be determined empirically.

Acknowledgements

References

1. Monod J, Wyman J, Changeux J-P (1965) On the nature of allosteric transitions: a plausible model. J Mol Biol 12:88–118

2. Koshland DE, Nemethy G, Filmer D (1972) Comparison of experimental binding data and theoretical models in proteins containing subunits. Biochemistry 5:365–385

3. Giedroc DP, Arunkumar AI (2007) Metal sensor proteins: nature's metalloregulated allosteric switches. Dalton Trans 29:3107–3120

4. Ma Z, Jacobsen FE, Giedroc DP (2009) Coordination chemistry of bacterial metal transport and sensing. Chem Rev 109:4644–4681

5. Busenlehner LS, Pennella MA, Giedroc DP (2003) The SmtB/ArsR family of metalloregulatory transcriptional repressors: structural insights into prokaryotic metal resistance. FEMS Microbiol Rev 27:131–143

6. Hobman JL, Wilkie J, Brown NL (2005) A design for life: prokaryotic metal-binding MerR family regulators. Biometals 18:429–436

7. Brown NL, Stoyanov JV, Kidd SP, Hobman JL (2003) The MerR family of transcriptional regulators. FEMS Microbiol Rev 27:145–164

8. Reinhart GD (2004) Quantitative analysis and interpretation of allosteric behavior. Methods Enzymol 380:187–203

9. Grossoehme NE, Giedroc DP (2009) Energetics of allosteric negative coupling in the zinc sensor *S. aureus* CzrA. J Am Chem Soc 131: 17860–17870. doi: 10.1021/ja906131b

10. Ma Z., Cowart DM, Ward BP, Arnold RJ, DiMarchi RD, Zhang L et al (2009) Unnatural amino acid substitution as a probe of the allosteric coupling pathway in a mycobacterial Cu

(I) sensor. J Am Chem Soc 131:18044–18045. doi: 10.1021/ja908372b

11. Singh VK, Xiong A, Usgaard TR, Chakrabarti S, Deora R, Misra TK et al (1999) ZntR is an autoregulatory protein and negatively regulates the chromosomal zinc resistance operon znt of Staphylococcus aureus. Mol Microbiol 33:200–207

12. Xiong A, Jayaswal RK (1998) Molecular characterization of a chromosomal determinant conferring resistance to zinc and cobalt ions in Staphylococcus aureus. J Bacteriol 180:4024–4029

13. Sun Y, Wong MD, Rosen BP (2001) Role of cysteinyl residues in sensing Pb(II), Cd(II), and Zn(II) by the plasmid pI258 CadC repressor. J Biol Chem 276:14955–14960

14. Lee JW, Helmann JD (2007) Functional specialization within the Fur family of metalloregulators. Biometals 20:485–499

15. Andrews SC, Robinson AK, Rodriguez-Quinones F (2003) Bacterial iron homeostasis. FEMS Microbiol Rev 27:215–237

16. Stoll KE, Draper WE, Kliegman JI, Golynskiy MV, Brew-Appiah RA, Phillips RK et al (2009) Characterization and structure of the manganese-responsive transcriptional regulator ScaR. Biochemistry 48:10308–10320

17. Payne JC, ter Horst MA, Godwin HA (1999) Lead fingers: Pb^{2+} binding to structural zinc-binding domains determined directly by monitoring lead-thiolate charge-transfer bands. J Am Chem Soc 121:6850–6855

18. Busenlehner LS, Weng TC, Penner-Hahn JE, Giedroc DP (2002) Elucidation of primary (a3N) and vestigial (a5) heavy metal-binding sites in Staphylococcus aureus pI258 CadC: evolutionary implications for metal ion selectivity of ArsR/SmtB metal sensor proteins. J Mol Biol 319:685–701

19. Busenlehner LS, Giedroc DP (2006) Kinetics of metal binding by the toxic metal-sensing transcriptional repressor Staphylococcus aureus pI258 CadC. J Inorg Biochem 100 (5–6):1024–1034

20. Magyar JS, Godwin HA (2003) Spectropotentiometric analysis of metal binding to structural zinc-binding sites: accounting quantitatively for pH and metal ion buffering effects. Anal Biochem 320:39–54

21. Good NE, Winget GD, Winter W, Connolly TN, Izawa S, Singh RMM (2002) Hydrogen ion buffers for biological research*. Biochemistry 5:467–477

22. Yu Q, Kandegedara A, Xu Y, Rorabacher DB (1997) Avoiding interferences from good's buffers: a contiguous series of noncomplexing tertiary amine buffers covering the entire range of pH 3–11. Anal Biochem 253:50–56

23. Hegetschweiler K, Saltman P (1986) Interaction of copper(II) with N-(2-hydroxyethyl) piperazine-N′-ethanesulfonic acid (HEPES). Inorg Chem 25:107–109

24. Record MT Jr, Ha JH, Fisher MA (1991) Analysis of equilibrium and kinetic measurements to determine thermodynamic origins of stability and specificity and mechanism of formation of site-specific complexes between proteins and helical DNA. Methods Enzymol 208:291–343

25. Chen X, Agarwal A, Giedroc DP (1998) Structural and functional heterogeneity among the zinc fingers of human MRE-binding transcription factor-1. Biochemistry 37:11152–11161

26. Ma Z, Cowart DM, Scott RA, Giedroc DP (2009) Molecular insights into the metal selectivity of the copper(I)-sensing repressor CsoR from Bacillus subtilis. Biochemistry 48:3325–3334

27. National Institutes of Standards and Technology (2003) NIST Standard Reference Database 46, Version 7.0

28. Eicken C, Pennella MA, Chen X, Koshlap KM, VanZile ML, Sacchettini JC et al (2003) A metal-ligand-mediated intersubunit allosteric switch in related SmtB/ArsR zinc sensor proteins. J Mol Biol 333:683–695

29. Busenlehner LS, Cosper NJ, Scott RA, Rosen BP, Wong MD, Giedroc DP (2001) Spectroscopic properties of the metalloregulatory Cd (II) and Pb(II) sites of S. aureus pI258 CadC. Biochemistry 40:4426–4436

30. Zheng M, Cooper DR, Grossoehme NE, Yu M, Hung LW, Cieslik M et al (2009) Structure of Thermotoga maritima TM0439: implications for the mechanism of bacterial GntR transcription regulators with Zn2 + -binding FCD domains. Acta Crystallogr D Biol Crystallogr 65:356–365

31. Cotton AW, Geoffrey M, Carlos A, Bochman M (1999) Advanced inorganic chemistry, 6th edn. Wiley, New York

32. Pennella MA, Arunkumar AI, Giedroc DP (2006) Individual metal ligands play distinct functional roles in the zinc sensor Staphylococcus aureus CzrA. J Mol Biol 356:1124–1136

33. Liu T, Golden JW, Giedroc DP (2005) A zinc (II)/lead(II)/cadmium(II)-inducible operon from the Cyanobacterium anabaena is regulated by AztR, an alpha3N ArsR/SmtB metalloregulator. Biochemistry 44:8673–8683

34. Frankel AD, Berg JM, Pabo CO (1987) Metal-dependent folding of a single zinc finger from transcription factor IIIA. Proc Natl Acad Sci U S A 84:4841–4845

35. VanZile ML, Cosper NJ, Scott RA, Giedroc DP (2000) The zinc metalloregulatory protein Synechococcus PCC7942 SmtB binds a single zinc ion per monomer with high affinity in a tetrahedral coordination geometry. Biochemistry 39:11818–11829

36. Walkup GK, Imperiali B (1997) Fluorescent chemosensors for divalent zinc based on zinc finger domains. Enhanced oxidative stability, metal binding affinity, and structural and functional characterization. J Am Chem Soc 119:3443–3450

37. Golynskiy MV, Gunderson WA, Hendrich MP, Cohen SM (2006) Metal binding studies and EPR spectroscopy of the manganese transport regulator MntR. Biochemistry 45:15359–15372

38. Jefferson JR, Hunt JB, Ginsburg A (1990) Characterization of indo-1 and quin-2 as spectroscopic probes for Zn^{2+}–protein interactions. Anal Biochem 187:328–336

39. VanZile ML, Chen X, Giedroc DP (2002) Structural characterization of distinct alpha3N and alpha5 metal sites in the cyanobacterial zinc sensor SmtB. Biochemistry 41:9765–9775

40. Liu T, Chen X, Ma Z, Shokes J, Hemmingsen L, Scott RA et al (2008) A Cu(I)-sensing ArsR family metal sensor protein with a relaxed metal selectivity profile. Biochemistry 47:10564–10575

41. VanZile ML, Chen X, Giedroc DP (2002) Allosteric negative regulation of smt O/P binding of the zinc sensor, SmtB, by metal ions: a coupled equilibrium analysis. Biochemistry 41:9776–9786

42. Lakowicz JR (1999) Principle of fluorescence spectroscopy. Kluwer Academic, New York

43. Arunkumar AI, Campanello GC, Giedroc DP (2009) Solution structure of a paradigm ArsR family zinc sensor in the DNA-bound state. Proc Natl Acad Sci U S A 106:18177–18182

44. Lee S, Arunkumar AI, Chen X, Giedroc DP (2006) Structural insights into homo- and heterotropic allosteric coupling in the zinc sensor S. aureus CzrA from covalently fused dimers. J Am Chem Soc 128:1937–1947

45. Chen X, Chu M, Giedroc DP (1999) MRE-Binding transcription factor-1: weak zinc-binding finger domains 5 and 6 modulate the structure, affinity, and specificity of the metal-response element complex. Biochemistry 38:12915–12925

46. Grossoehme NE, Li L, Keane SC, Liu P, Dann CE 3rd, Leibowitz JL et al (2009) Coronavirus N protein N-terminal domain (NTD) specifically binds the transcriptional regulatory sequence (TRS) and melts TRS-cTRS RNA duplexes. J Mol Biol 394:544–557

47. Busenlehner LS, Apuy JL, Giedroc DP (2002) Characterization of a metalloregulatory bismuth(III) site in Staphylococcus aureus pI258 CadC repressor. J Biol Inorg Chem 7:551–559

48. Ye J, Kandegedara A, Martin P, Rosen BP (2005) Crystal structure of the Staphylococcus aureus pI258 CadC Cd(II)/Pb(II)/Zn(II)-responsive repressor. J Bacteriol 187:4214–4221

49. Apuy JL, Busenlehner LS, Russell DH, Giedroc DP (2004) Ratiometric pulsed alkylation mass spectrometry as a probe of thiolate reactivity in different metalloderivatives of Staphylococcus aureus pI258 CadC. Biochemistry 43:3824–3834

50. Kuzmic P (1996) Program DYNAFIT for the analysis of enzyme kinetic data: application to HIV proteinase. Anal Biochem 237:260–273

51. Johnson ML, Faunt LM (1992) Parameter estimation by least-squares methods. Methods Enzymol 210:1–37

52. Lohman TM, Bujalowski W (1991) Thermodynamic methods for model-independent determination of equilibrium binding isotherms for protein–DNA interactions: Spectroscopic approaches to monitor binding. Methods Enzymol 208:258–290

53. Pennella MA, Shokes JE, Cosper NJ, Scott RA, Giedroc DP (2003) Structural elements of metal selectivity in metal sensor proteins. Proc Natl Acad Sci U S A 100:3713–3718

54. Cleland WW (1964) Dithiothreitol, a new protective reagent for SH groups. Biochemistry 3:480–482

55. Krezel A, Lesniak W, Jezowska-Bojczuk M, Mlynarz P, Brasuñ J, Kozlowski H et al (2001) Coordination of heavy metals by dithiothreitol, a commonly used thiol group protectant. J Inorg Biochem 84:77–88

56. Millis KK, Weaver KH, Rabenstein DL (1993) Oxidation/reduction potential of glutathione. J Org Chem 58:4144–4146

57. Mayhew SG (1978) The redox potential of dithionite and SO-2 from equilibrium reactions with flavodoxins, methyl viologen and hydrogen plus hydrogenase. Eur J Biochem 85:535–547